Size-Dependent Transport Characteristics of Ballistic Silicon Nanowire FETs

Yeonghun Lee[1], Kuniyuki Kakushima[2], Kenji Shiraishi[3], Kenji Natori[1] and Hiroshi Iwai[1]
Tokyo Institute of Technology, [1]Frontier Research Center, [2]Interdisciplinary Graduate School of Science and Eng., Electronics and Applied Physics
4259-S2-20 Nagatsuta, Midori-ku, Yokohama 226-8502, Japan
[3]Univ. of Tsukuba, Graduate School of Pure and Applied Sciences, 1-1-1 Tennodai, Tsukuba 305-8571, Japan

Introduction: From scaling limit issues in planar MOSFETs, 3D MOSFETs including a FinFET have been focused for future LSI devices, owing to their ability to reduce the off-current (I_{OFF}), which eventually reduce power consumption. These 3D-MOSFETs also provide the large on-current (I_{ON}) by adjusting the threshold voltage (V_{th}) to appropriate values. However, the total current required for driving the circuit would be limited owing to their narrow cross section. This concern is also applied to nanowire FET, which is the ultimate 3D MOSFET. Although the nanowire FET has a smaller cross section, a large I_{on} can be obtained with reduced scattering by its short channel immunity. In this study, size-dependent band structures of silicon nanowires (SiNWs) are calculated by first principles calculation. And, size-dependent ballistic transport characteristics of the SiNW FETs are calculated using derived band structures.

Methods: The band structures of SiNWs were calculated by first principles calculation on the basis of density functional theory (DFT) with local density approximation (LDA) using pseudopotential. All the calculations are done by Tokyo Ab-initio Program Package (TAPP). The shape of SiNWs is modeled as a square pillar, which aligned along [100] direction, and calculated SiNWs had various width w_{SiNW} ranging from 0.77 to 2.69 nm. Dangling bonds of peripheric atoms are passivated by hydrogen atoms. The pseudopotentials are made by cutoff radii of wave functions of silicon and hydrogen electrons set by 2.2 and 0.7 a.u., respectively. The cutoff energy was set to 12.25 Ry. As a periodic boundary condition for adopting super cells, neighboring wires were separated by 0.7 nm. Brillouin zone integral was done by two sample k points. From the calculated band structures, ballistic transport characteristics of SiNW FETs were derived on the basis of the one-dimensional ballistic transport model proposed by Natori.[1] The transport parameters were derived at temperature of 300 K with gate overdrive ($V_g - V_{th}$) of 1.0 V and drain voltage of 1.0 V enough to saturate drain current I_d as which I_d is I_{ON}. A cylindrical wire model having the same cross-sectional area as the square cross section of the SiNW adopted for band structure calculation is assumed, and 1-nm-thick SiO_2 is adopted as a gate insulator.

Results: Figure 1 shows the band structures of [100] SiNWs with w_{SiNW} of 0.77 and 2.69 nm. Direct bandgaps at the Γ point are obtained for both SiNWs, which is in contrast to the bandgap for bulk silicon. Valley splitting of the four unprimed minima occurs while they are in a state of 4-fold degeneracy in a sufficiently large wire. One of the noticeable evolutions with w_{SiNW} is that a primed subband moves toward lower unprimed subband minima, which have a strong effect on the ballistic I_{ON}. Figure 2 shows size-dependent electron effective masses m^* of the lowest unprimed and primed subbands. m^* becomes light as w_{SiNW} increases in both the lowest unprimed and primed subbands. Size-dependent i-th subband minima E_{imin} and source Fermi level μ_s are shown in fig. 3. μ_s increases as w_{SiNW} increases, and gradually saturates in large wires. Here, μ_s is determined by the balance between density of states (DOS) and effective capacitance C_{eff}, both of which increase as wire size increases. μ_s of a yet larger wire is expected to decrease owing to sinking of the upper subbands, which have larger degeneracy and DOS. Figure 4 shows linear charge density $|Q|$ of each subband versus w_{SiNW}. The linear gate capacitances C_g are almost proportional to w_{SiNW}, as excepted. In fact, ($V_g - V_{th}$) is not completely applied to the nanowire channel because of the series connection of quantum capacitance C_q. On this account, C_{eff}, which denotes the effective capacitance for the same ($V_g - V_{th}$), is smaller than C_g. The charge in the unprimed subband is almost constant for w_{SiNW} larger than 1.54 nm, and excess charge is stored in primed and other higher subbands. Figure 5 shows saturation mean velocity v_{sat} of charge stored in each subband versus w_{SiNW}. The v_{sat} of the primed subband is much smaller than v_{sat} of the unprimed subbands, and both of them increase as w_{SiNW} increases. The increase of both v_{sat} is also caused by the sinking of E_{imin} below μ_s and the decrease of m^*. Multiplying the extracted $|Q|$ and v_{sat}, I_{ON} is obtained as shown in fig. 6. A large I_{ON} is obtained from large SiNWs because the increase of linear capacitance is more dominant for current increase than the variation of all subband v_{sat} values.

Conclusions: Size-dependent band structures of [100]-directed SiNWs with the width ranging from 0.77 to 2.69 nm have been calculated by first-principles calculation. The prominent features of SiNWs are the increase in band splitting and effective mass as width increases. Ballistic drain current estimations from the calculated band structures have revealed that subband structure and parameters that contribute to the on-current evolution have been clarified by systematic analyses. Finally, the on-current steadily increases with large wire size owing to the increase in linear charge density despite the peaked saturation mean velocity of the all subbands.

Reference

[1] K. Natori: IEEE Trans. Electron Devices **55** (2008), 2877.

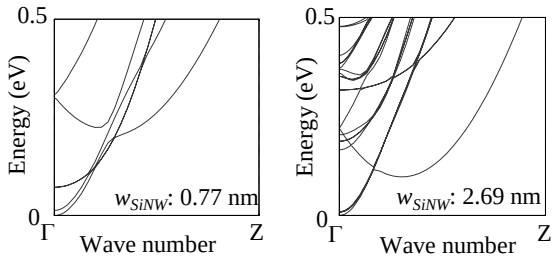

Fig. 1 Band structures of [100] SiNWs with w_{SiNW} of 0.77 and 2.69 nm. The longitudinal axes indicate relative values from each band edge.

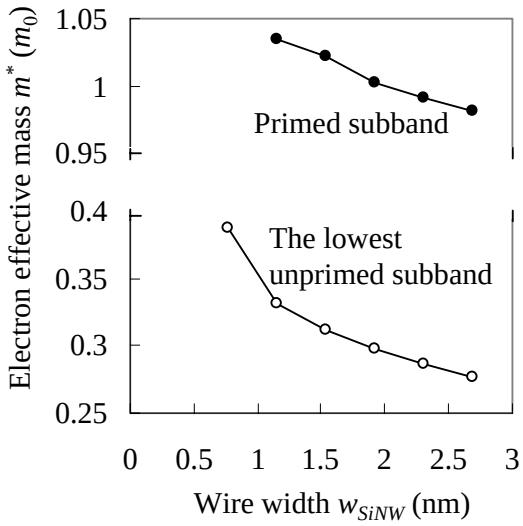

Fig. 2 Upper solid circles indicate w_{SiNW} dependent m^* of primed subband and lower open circles indicate those of the lowest unprimed subband. Both decrease as w_{SiNW} increases.

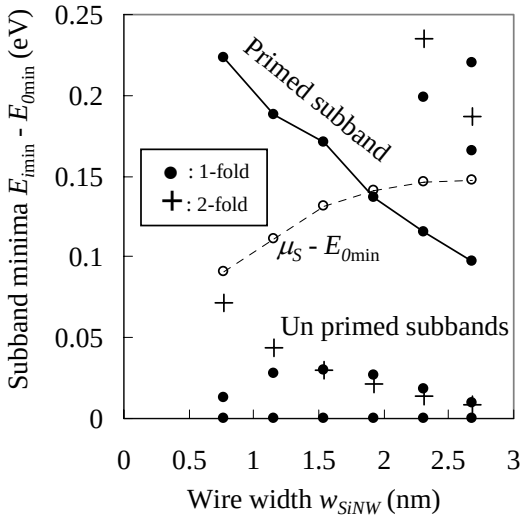

Fig. 3 w_{SiNW} dependences of E_{imin} and μ_s based on E_{0min}. Solid circles (cross point) indicate 1-fold (2-fold) degenerate subband minima. Primed subband minima are connected by solid line. Open circles with dotted line indicate μ_s. Evolution of primed subband minima and μ_s are important to investigation of I_{ON}.

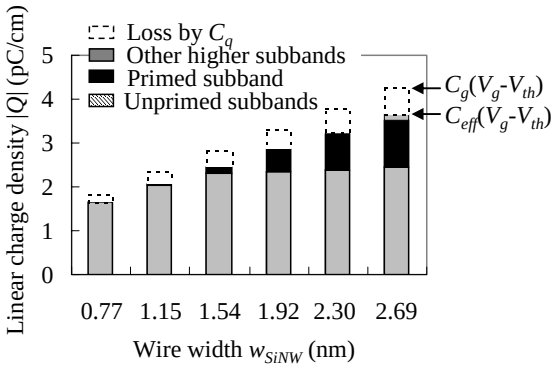

Fig. 4 w_{SiNW} dependences of $|Q|$ of each subband. Top of the bars indicates $C_g(V_g - V_{th})$. The $C_{eff}(V_g - V_{th})$ is represented by other bars, except open dotted square, which represents loss by C_q. Hatched, black and grey areas indicate linear charge density in unprimed, primed and other higher subbands, respectively.

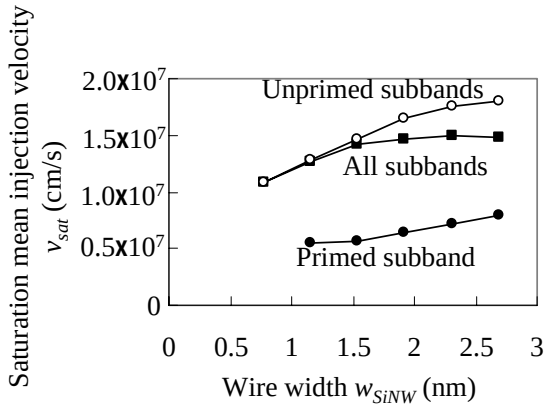

Fig. 5 w_{SiNW} dependences of v_{sat} of each subband. Solid squares, open circles and solid circles indicate v_{sat} of all subbands, unprimed subbands and primed subband, respectively. The v_{sat} of all subbands reaches a peak at w_{SiNW} of 2.30 nm.

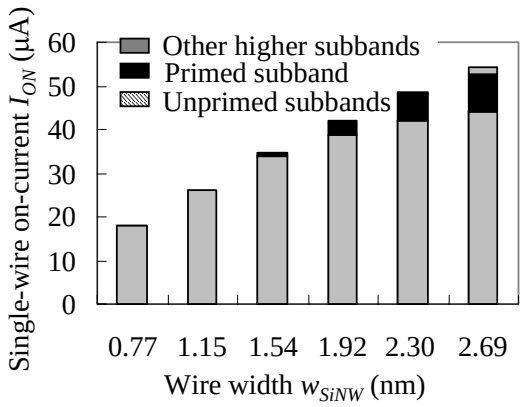

Fig. 6 w_{SiNW} dependences of I_{ON} of each subband. Top of the bars indicates the total I_{ON}. Hatched, black and grey areas indicate contributions of on-current of unprimed, primed and other higher subbands to total I_{ON}, respectively.